



Rapid Synthesis of Metal Nanoparticles Using Low-Temperature, Low-Pressure Argon Plasma Chemistry and Self-Assembly

Journal:	<i>Green Chemistry</i>
Manuscript ID	GC-ART-07-2022-002592.R2
Article Type:	Paper
Date Submitted by the Author:	19-Aug-2022
Complete List of Authors:	Traba, Christian; Fairleigh Dickinson University Darwish, Marjan; Fairleigh Dickinson University Mafla-Gonzalez, Camila; Fairleigh Dickinson University kolenovic, Belmin; Fairleigh Dickinson University Deremer, Adrianna; Fairleigh Dickinson University Centeno, Daniel; Stevens Institute of Technology Liu, Tianchi; Fourth State of Matter Technologies Kim, Deok-Yang; Bergen County Technical School District Adult and Continuing Education Cattabiani, Thomas; Fourth State of Matter Technologies Drwiega, Thomas; Fairleigh Dickinson University Kumar, Ish; Fairleigh Dickinson University Li, Clive; Hudson County Community College

Rapid Synthesis of Metal Nanoparticles Using Low-Temperature, Low-Pressure Argon Plasma Chemistry and Self-Assembly

Marjan Darwish¹, Camila Mafla-Gonzalez¹, Belmin Kolenovic¹, Adrianna Deremer¹, Daniel Centeno³, Tianchi Liu³, Deok-Yang Kim⁴, Thomas Cattabiani³, Thomas J. Drwiega¹, Ish Kumar¹, Clive Li², and Christian Traba^{1*}

First three authors contributed equally to this work.

Department of Chemistry, Biochemistry and Physics, Fairleigh Dickinson University,
Teaneck, NJ 07666, USA¹

Department of STEM, Hudson County Community College, Jersey City, NJ 07306, USA²

Fourth State of Matter Technologies Corporation, Bayonne, NJ 07306, USA³

Bergen County Technical Schools, Hackensack, NJ 07601, USA⁴

* Corresponding author

Dr. Christian Traba

Department of Chemistry, Biochemistry and Physics

Fairleigh Dickinson University

Teaneck, NJ 07666, USA

Tel.: 201-696-2526; Fax: 201-696-7349

Email: ctraba@fdu.edu

Abstract

The synthesis of metal nanoparticles has become a priority for the advancement of nanotechnology. In attempts to create these nanoparticles, several different methods: chemistry, physics, and biology, have all been used. In this study, we report the reduction of cations using argon plasma chemistry to produce nanoparticles of gold (AuNPs), silver (AgNPs), and copper (CuNPs). Although other groups have used plasma-reduction methods to synthesize metal nanoparticles from their cation counterparts, these approaches often require plasma|liquid state interactions, high temperature, specific combinations of gases, and extended treatment times (>10 minutes), for which only specific cations (noble or non-noble) may be reduced. As a result, we have developed a non-thermal, low-pressure argon-plasma|solid state approach for the reduction of both noble and non-noble cations. More specifically, when 50- μ L droplets of 2-mM solutions of gold(III) chloride, silver nitrate, or copper(II) sulfate are exposed to vacuum, they undergo an evaporation process. As the pressure in the chamber decreases to 220 mtorr, the droplets become completely evaporated, leaving behind a metal precursor. Nucleation and growth studies reveal that when the metal precursors of gold(III) chloride, silver nitrate, and copper(II) sulfate are treated with 80 watts of argon plasma for 5, 60, and 150 seconds, respectively, nanoparticles could be synthesized with efficiency rates of upwards of 98%. The size of nanoparticles synthesized in this work was studied using Scanning Electron Microscopy, and the scattering properties of the nanoparticles was studied using UV/Vis spectroscopy. Transmission Electron Microscopy with corresponding elemental analysis was also very useful in confirming the identity of the synthesized nanoparticles. The results from this study reveal that we have synthesized metal nanoparticles with distinct chemical and

physical properties. Scanning Electron Microscopy depicts AgNPs with a round-shape and diameters from 40 - 80 nm, while AuNPs were hexagonal, with sizes from 40 - 80 nm, and CuNPs were rod-shaped, with dimensions 40 by 160 nm. Our findings demonstrate that the argon plasma approach used in this study is a rapid, green, and versatile reduction method for the synthesis of both noble and non-noble metal nanoparticles.

Keywords: Plasma reduction; silver; copper; gold; nanoparticles.

Abbreviations: UV/Vis: Ultraviolet Visible Spectroscopy; NP: Nanoparticle; SEM: Scanning Electron Microscopy; TEM: Transmission Electron Microscopy; PET: Polyethylene Terephthalate; AgNPs: Silver Nanoparticles; AuNPs: Gold Nanoparticles; CuNPs: Copper Nanoparticles

1. Introduction

Advances in nanotechnology, with particular emphasis on nanoparticles of silver (AgNPs), gold (AuNPs), and copper (CuNPs), have opened new avenues in disease diagnosis and treatment, cancer therapy, drug delivery, and antimicrobial coatings.^[1-5] Aside from their therapeutic applications, the non-therapeutic applications of these nanoparticles (NPs) utilize their electrical, catalytic, and optical properties, which are commonly used in circuits and biosensing platforms. It is believed that their high surface area, optical, electronic, and magnetic, properties, antimicrobial activity and unique physicochemical characteristics, including catalytic activity, make NPs very interesting candidates across a very broad range of applications.^[6-10] In addition, the highly energetic

electrons in plasmas are also used to induce the conversion of CH₄ and CO₂ into useful compounds such as urea and alcohols.^[11,12] With that being said, NPs have been studied extensively and are widely accepted to exhibit different properties for many different applications.^[13-15] Nanoparticles are often synthesized using different approaches, ranging from chemical, physical, to biological methods.^[16-24] As a result, these different approaches lack a homogeneous product, and often result in different chemical and physical properties.^[1-7]

The most common approach for the synthesis of NPs is through wet chemistry, in which butylamine, hydrazine, sodium hypophosphite, and other chemicals such as sodium tetrahydridoborate act as the reducing agent. However, this approach has serious negative implications on the environment.^[25,26] As a result, alternative strategies have been attempted, including electrochemical reduction, laser ablation, and photocatalytic reduction using UV irradiation.^[13,14] Unfortunately, these reduction approaches also require a chemical reducing agent and have negative implications for the environment.^[25,26] Consequently, alternative reduction technologies have attracted much attention and include plasma technology reduction and the self-assembly approach.^[13,14] The self-assembly approach begins at the atomic level. These atoms, when subjected to an electric field can spontaneously organize into ordered nanomaterials including nanoparticles, nanorods, or even nanopatterns.^[27-30] This is accomplished through different chemical forces such as chemical bonds and van der Waals forces.

The synthesis of NPs involving the plasma|liquid approach was introduced more than a century ago and has become revitalized over the past two decades.^[31-41] This field includes three categories: (1) direct liquid phase discharges; (2) discharges in the gas phase

with liquid electrode(s), and (3) discharges in bubbles in liquids.^[42] These types of electrochemical reactions are performed using aqueous electrolytes, molten salts or ionic liquids.^[38-43] In all of these techniques, the chemistry takes place between the electronic conductor (electrodes) and the ionic conductor (electrolyte), with charge transfer across the interface.^[38] Due to the complexity of the chemistry and physical properties at the plasma|liquid interface, this interaction is not completely understood.^[31]

Different types of plasmas and plasma devices have been reported to reduce of metal cations to metal NPs.^[6,22,23] However, these different systems operate under all different temperatures and pressures in comparison to our system. Early reduction of cations using plasma technology began with hydrogen plasma, as it was believed that only hydrogen plasma could produce the species required for reduction.^[6] With time, this approach evolved into the application of mixing different types of plasmas for the reduction of noble cations.^[24] Eventually, it became apparent that the plasma reduction process does not require only highly reactive hydrogen species to reduce cations. In fact, plasmas from inert gases such as argon and helium are capable of reducing these cations, and do not have those hydrogen species.^[23-24]

Work in our lab has resulted in the formation of metal NPs within 150 seconds of treatment with low pressure, low-temperature argon plasma. To achieve this, 2 mM solutions of either gold(III) chloride, silver nitrate, or copper(II) sulfate, were pipetted onto a sample holder, making up to 72 droplets with volumes of 50 μL . These droplets were then subjected to vacuum, resulting in evaporation, thus leaving behind the salt, which we call metal precursors. These precursors were then treated with argon plasma under specific conditions. This argon plasma produces ample concentration of electrons, along with

different excited argon species that become reducing agents. These species help to accelerate the transformation of both noble, and non-noble cations to NPs, thus shortening the reaction time. This approach proves to be rapid, green, and versatile for the synthesis of both noble and non-noble metal NPs.

2. Materials and methods

2.1 Materials

The substrates used to support the different droplets include polyethylene terephthalate (PET) films, purchased from Goodfellow Corporation (Coraopolis, PA USA), petri dishes, purchased from USA Scientific (Ocala, FL USA), 6-well plates, purchased from USA Scientific (Ocala, FL USA), and silicon wafers, purchased from University Wafer (South Boston, MA USA).

2.2. Reagents and solutions

Gold(III) chloride trihydrate, silver nitrate, and copper(II) sulfate pentahydrate, all of >99% purity were purchased from Sigma-Aldrich (Milwaukee, WI, USA). All solution preparation and glassware cleaning procedures used ultrapure (Milli-Q) water (resistivity 18.2 M Ω).

2.3. Generation of gas discharge plasma

Argon plasma was produced using a Plasma Prep III device from SPI Supplies (West Chester, PA). This plasma device is operated under vacuum and contains a reactor comprising a pyrex glass chamber (10.45 cm in diameter) and a pair of electrodes (an upper and lower electrode). A radiofrequency generator was supplied with a frequency of 13.56 MHz and had an output of up to 100 W (Fig. 1). The system was evacuated to a working pressure of 220 mtorr while argon gas was introduced to the chamber at a flow rate of 2.4

ft³/hr. Bottled argon was purchased from Praxair (Keasbey, NJ, USA) and was prepared by Cryogenic Air separation, which led to purity of > 99.9%.

2.4. Plasma reduction process

After the 2 mM aqueous solutions of gold(III) chloride (Fig. 2X), silver nitrate (Fig. 2Y), and copper(II) sulfate (Fig. 2Z) were prepared, 72 droplets, with a volume of 50 μ L each, were pipetted onto the sample holder (PET films, polyethylene petri dishes, polyethylene 6-well plates, or silicon wafers), as shown in Fig. 2A. Once placed inside the plasma chamber (Fig. 2B) and subjected to the vacuum, the droplets underwent a solvent evaporation process (Fig. 2C). This process required 3 minutes of vacuum exposure. Once the solvent evaporation was complete, the chamber reached a pressure of 220 mtorr, leaving behind the salt or what we refer to as the metal precursor (Fig. 2D). At 220 mtorr, the samples were treated with optimal experimental conditions (Fig. 2E), and NPs were synthesized (Fig. 2F). After reduction, the sample holders were removed, and images of the NPs were taken against a white background (Fig. 2G). Standard deviation bars were calculated using at least 100 plates, each containing the 72 droplets. The sample holders were placed approximately 8 cm away from the discharge gas outlet.^[44-48] The purpose of the experiment determined which sample holder would be used, along with the number of drops that would be pipetted onto the sample holder. Exposure of the metal precursor to argon plasma is essential for reducing cations. The chamber pressure was maintained at 220 mtorr with a working temperature of about 40 - 60°C. Due to manufacturing settings the plasma chamber is under vacuum and therefore isolated from the environment, resulting in no, or very minimal, plasma chamber contamination.^[44-48]

2.5. Nanoparticle washing

The synthesized metal NPs were washed three times with Milli-Q water by ultracentrifugation (30,000 rpm, 60 min). After the washing step, each batch of NPs was then collected by ultracentrifugation.^[44,48]

2.6. Characterization of metal nanoparticles

Characterization of the argon-plasma-induced synthesis of NPs was first carried out using a Cary 60 UV-visible spectrophotometer (Agilent Technologies). The UV/Vis was conducted in the absorbance mode in the range of 300–900 nm with a micro-quartz cuvette.

In addition, the shape and size of the three different types of NPs were studied using an Auriga Scanning Electron Microscope (SEM). The synthesized NPs (35 mg) were first washed and then placed into 10 mL of milli-Q water. The prepared solutions were then diluted 1,000 times. From the diluted solutions, 4 μ L of the solution was pipetted onto a silicon wafer for SEM imaging or onto a 300 mesh copper TEM grid (Electron Microscopy Sciences, Q325-CMA) for TEM elemental analysis. Solutions were allowed to adhere onto the substrates for 4 hours. This dilution protocol was used to reduce NP aggregation.^[44] By achieving this, we could optimize our system and observe highly magnified images of our NPs. At least ten SEM images of each sample were taken to obtain a representative assessment of the size of the different particles in the sample. With regards to TEM elemental analysis, different spots on the copper TEM grid were located and elemental analysis of NPs were obtained by the image processing software EDAX Team EDS.

2.7. Collection of nanoparticles

The efficiency of metal NPs synthesized from argon plasma-reduction was determined using an analytical balance. To accomplish this, large quantities (>3 mg) of NPs had to be synthesized in order to accurately weigh out the NPs. In these experiments, five batches

possessing the 72 droplets were combined, washed, and dried under nitrogen at 35 °C. The difference between the theoretical amount and the actual amount of NPs synthesized and collected under different experimental conditions was determined. From this, we were able to calculate that the loss of NPs after plasma reduction and sample washing was about 3%. This loss in sample was taken into consideration for all studies involving the optimization of plasma reduction conditions. The theoretical mass of 72 drops of 50 μL for Ag^+ , Au^{3+} , and Cu^{2+} was calculated to be 0.7762 mg, 1.412 mg, and 0.4575 mg, respectively. These amounts were calculated using stoichiometric conversions.

3. Results and discussion

3.1. Non-thermal reduction of metal ions

There are many different types of methods to produce NPs from atoms, ions and molecules. These processes occur from transformations in solution involving photodeposition, sol-gel processing, chemical vapor deposition (CVD), plasma or flame spraying synthesis, laser pyrolysis, atomic or molecular condensation.^[49,50] However, these chemical processes rely on the availability of appropriate “metal-organic” molecules as precursors. In this study, we use a low-temperature, low-pressure argon plasma reduction of cations and then self-assembly to synthesize NPs directly from their ionic form. This approach can be tailored to produce various types of NPs, and NP sizes depending on the chemical composition, and the amount of metal precursors that are initially utilized during the reduction.

Argon plasma technology, was used for every step of the NP synthesis process (Fig. 3). This includes catalyst preparation through etching, decomposition, oxidation, or reduction.^[31-33,43] In this study, three chemically different metal precursors in solution,

were pipetted onto sample holders (Fig. 3A), and these droplets were exposed to a vacuum (Fig. 3B). During this time, solvent was evaporated from the droplets (Fig. 3C). At chamber pressures of roughly 220 mtorr, when evaporation was complete (Fig. 3D), the sample was treated with low-temperature, low-pressure argon plasma (Fig. 3E). From this, NPs were synthesized with specific size, shape, and color (Fig. 3F). It should be stated that at this plasma|solid interface, the reduction mechanism is not completely understood and several factors including sample substrate, the type of plasma device, and the working gas, must all be considered when attempting to decipher the reduction mechanism.^[31-33] In addition, the difficulty involved in studying the composition of the plasma prevents a complete and thorough analysis.^[37,51-58] With that being said, at this plasma|solid interface, it is presumed that the electrons play the most important role in the reduction of metal ions and are most likely the reducing agent when noble gases are used as the working gas.^[48,56,57] It is also accepted that some excited argon species generated by the electron-induced reactions can also be effective and efficient reducing agents.^[57]

Argon plasma treatment had significant effects on the colors observed from the NPs after treatment, giving AgNPs a gray color, AuNPs a dark blue/gray color, and CuNPs a dark yellow/brown color (Fig. 4A). These images were taken after the NPs were collected from the sample holder, washed, and then placed into 2 mL of water, forming a colloidal solution. (Fig. 4A). Characteristic changes in color were observed during treatment. For example, the 2 mM solution of AgNO₃ started as colorless (Fig. 4B_L), but when the 72 droplets (50 μL) were placed inside the plasma chamber and exposed to the vacuum, the evaporation process began. At a pressure of around 220 mtorr, evaporation was complete, and a white metal precursor appeared. After optimal plasma treatment (80 W of argon

plasma for 60 sec), the white metal precursor changed to a silver color (Fig. 4B_R). The 2 mM solution of HAuCl₄ started as pale-yellow (Fig. 4C_L), and when the 72 droplets (50 μL) were placed inside the plasma chamber and exposed to the vacuum, the evaporation process began. At a pressure of around 220 mtorr, evaporation was complete, and a yellow metal precursor appeared. After optimal plasma treatment (80 W of argon plasma for 5 sec), the yellow color changed to a dark blue/gray (Fig. 4C_R). When dealing with the 2 mM solution of CuSO₄ the solution started as colorless (Fig. 4D_L). However, when the solvent was evaporated in the plasma chamber, a white metal precursor appeared. After optimal plasma treatment (80 W of argon plasma for 150 sec), the white color changed to a dark yellow/brown color (Fig. 4D_R). These color changes provided the initial evidence of the chemical reduction of the cations to the metal NPs.

3.2. Optimization of argon plasma reduction

Effects from argon plasma power (Fig. 5A), and argon plasma treatment time (Fig. 5B), were evaluated with respect to each cation. In order to accurately assess the results generated from these experiments, the theoretical mass of each metal was calculated for each trial and was compared to the actual mass recorded after plasma reduction, washing, and collection. In these experiments, an analytical balance was used to measure the amounts of NPs collected and compare them to the theoretical yield. When studying the effects from plasma power (Fig. 5A), it was imperative that we keep the concentration of the salt solutions fixed at 2 mM and the argon plasma treatment times fixed at 5, 60 and 150 seconds for gold, silver, and copper. Results from this study typically followed a bi-phasic curve, and as expected, increasing plasma discharge powers positively affected the production of metal NPs. More specifically, at 60 W, significant amounts (>40%) of NPs

could be synthesized, and when plasma powers approached 80 W, optimal amounts (98%) of NPs were produced. However, when powers of more than 80 W were tested, a significant decrease (>17%) in the amounts of NPs synthesized were observed in both AgNPs and CuNPs. These results can be explained by the etching effects commonly associated with our plasma device.^[44-48] Unlike AgNPs and CuNPs, AuNPs formed at 100 W did not experience any loss in AuNPs because this etching effect is not significant until after 30 seconds of exposure (Data not shown).

The degree of NP synthesis was also dependent on plasma treatment times (Fig. 5B). In these experiments, the concentration of the cations was fixed to 2 mM and the argon plasma power was set to 80 W. These experimental conditions were chosen because at 80 W significant amounts (98%) of NPs could be synthesized (Fig. 5A). When testing the effects from argon plasma treatment times for the three different cations, some very interesting differences were observed. For example, the reduction of AuCl_4^- to Au^0 was extremely quick and reached optimal synthesis (98%) at 5 seconds of argon plasma treatment. The reduction of Ag^+ to Ag^0 followed a steady increase, in which less than half (48%) of NPs could be synthesized after 45 seconds of treatment. At 60 seconds of treatment, roughly 98% of NPs could be synthesized. Interestingly, the reduction of Cu^{2+} to Cu^0 followed a more gradual increase, and required the longest induction time (150 seconds) to reach complete reduction. In the case for all three cations, extended treatment times beyond the indicated optimal exposure had limited effects on the amount, size, and shape of NPs that were collected.

3.3. Effects from argon plasma power and treatment time

Effects from plasma power and plasma treatment time were important to understanding the nucleation and crystal growth involved in the synthesis of NPs. For example, the concentration and amount of energy possessed by the electrons and excited argon species produced at argon plasma powers (<60 W) were not capable of completely reducing the cations. In addition, limited plasma treatment times were unable to reduce all of the cations on the sample holder. We believe that the results obtained from nucleation and crystal growth studies are dependent on the reduction potentials for each of these cations. For example, the standard reduction potential for $\text{AuCl}_4^- + 3\text{e}^- \longrightarrow \text{Au}^0 + 4\text{Cl}^-$ is 1.0 V, while the value for $\text{Ag}^+ + \text{e}^- \longrightarrow \text{Ag}^0$ is 0.80 V, and for $\text{Cu}^{2+} + 2\text{e}^- \longrightarrow \text{Cu}^0$ is 0.34 V. These differences in potentials begin to provide a possible explanation for the results observed in nucleation and crystal growth studies, and demonstrate why the Au^{3+} ion required the shortest treatment time (5 seconds) for reduction, followed by Ag^+ (60 seconds), and then Cu^{2+} (150 seconds) when plasma power and solution concentrations were both fixed.

3.4. Characterization of nanoparticles

The absorbance from the AgNPs synthesized throughout this study was observed around 420 nm and demonstrates the successful synthesis of AgNPs (Fig. 6A).^[47] According to SEM imaging, the AgNPs had a round shape and had an average recorded size between 40 and 80 nm (Fig. 6D). There were some instances of AgNP aggregates, which could be found at be upwards of 100 nm. The absorbance from the AuNPs synthesized throughout this study was observed around 560 nm and these results confirm the presence of AuNPs (Fig. 6B).^[52] Corresponding SEM images depict AuNPs with an average size ranging from 40 – 80 nm, all with a hexagonal shape (Fig. 6E). This hexagonal

shape has also been seen by other groups, but while using a different approach.^[53] In some cases, AuNP aggregates were found to be upwards of 100 nm. Copper nanoparticles absorbed in the range of 780 nm (Fig. 6C). This absorption peak is not in agreement with literature, but can be explained by the size, color of solution that was produced, and by the shape of the NPs.^[14,15,53] Scanning Electron Microscopy depicts CuNPs with a rod-shape and a size of approximately 40 by 160 nm (Fig. 6F). From this work we report, for the first time, the synthesis of rod-shaped NPs using low-temperature, low pressure argon plasma chemistry and self-assembly. Corresponding TEM elemental analysis (Fig. 7), was useful in confirming the chemical identity of the metal NPs synthesized in this study and support the findings from both SEM and Ultraviolet-visible spectroscopy. It should be mentioned that since images were taken of the nanoparticles, our EDX analysis easily picked up information from the copper TEM plate, and introduced some false peaks into our analysis. With that in mind, elemental analysis of the AgNPs (Fig. 7A) identifies silver as the major product, since the Cu peak stems from the copper TEM grid. Elemental analysis of the AuNPs (Fig. 7B) identifies copper from the copper TEM grid as the major species and gold as the second major species. Since the copper absorption peak stems from the copper TEM grid, that makes gold the major component of the NPs. Analysis of the CuNPs (Fig. 7C) identifies copper as the major product of the NPs. As a result, we can confidently state that we have produced AgNPs, AuNPs, and CuNPs.

3.5. Effects of droplet concentration and droplet volume on nanoparticle synthesis

The quantity and quality of NPs synthesized in this study was dependent on the amount of metal precursor introduced into the plasma system. To better understand this, we studied how droplet concentration (Fig. 8A) and droplet volume (Fig. 8B) affected the synthesis of

NPs. When droplets were fixed to volumes of 50 μL , droplet concentration clearly affected the efficiency of NP synthesis (Fig. 8A). Interestingly, the synthesis of both AgNPs and AuNPs was efficient ($>87\%$), up until droplet concentrations of 40 mM silver nitrate or gold(III) chloride were used. In this range of droplet concentrations, the size and shape of the NPs that were synthesized were consistent with NPs produced using 2 mM concentrations. However, at droplet concentrations above 40 mM, the size of both AgNPs and AuNPs increased to the micro-range (Fig. 8C). In addition, at these higher droplet concentrations, the shapes of these particles began to change when compared to their nano-size counterparts (Fig. 8C). For example, AuNPs were more of a round shape. These changes are a direct result of the amounts of metal precursors at the beginning of plasma exposure. When dealing with CuNP synthesis, efficiency rates were high (92%) up until droplets of 20 mM were used. However, when concentrations of >20 mM were used, NP efficiency rates were reduced to 52%. It is likely that when these larger amounts of metal precursor were used, neither the excited argon species nor the electrons possessed enough energy to penetrate deep into the bulk of the sample for complete reduction (Data not shown). As a result, only the cations at the plasma|solid interface could be reduced. From these studies it can be deduced that argon plasma treatment controls NP shape, while precursor amounts controlled NP efficiency rates, NP size, NP aggregation, and NP growth. When summarizing the results from NP synthesis studies, it was observed that when 50- μL droplets with concentrations ranging from 2 through 40 mM for HAuCl_3 or AgNO_3 were used, and then treated under optimal reduction conditions, the diameters and distribution of the NPs were consistent at around 40 – 80 nm for both AuNPs and AgNPs (Table 1). Droplet concentrations of more than 40 mM resulted in much larger (>300 nm)

NPs (Table 1). In some cases, the size of the particles reached 1 μm . With respect to CuNPs, the average rod shapes were 40 x 160 nm up until concentrations of 20 mM were used. Beyond 20 mM, considerable increases in size were observed. In these cases, the sizes of the NPs increased almost three times from 40 x 160 nm to 100 x 500 nm (Table 1). Similar to both AuNPs and AgNPs, the sizes of the CuNPs consistently increased with respect to droplet concentration. The increase in concentration brings more precursor molecules, which increases the intensity of self-assembly during the nucleation process by introducing more building blocks that lead to bigger particles.

When droplet concentrations were fixed to 2 mM and droplet volumes were gradually increased from 50 to 1000 μL , the effects on NP synthesis became noticeable at larger volumes (Fig. 8B). Increases from 50 to 500 μL had limited effects on the efficiency of the NP synthesis (>92%), and the NPs that were synthesized possessed uniform size and shape when compared to NPs synthesized using 50 μL droplets. However, decreases in efficiency rates (78%) were observed when >750 μL droplets were pipetted on to the sample holder. Although these starting materials could be reduced, the size of the particles was measured at the micro-range. It was also interesting to see that the shapes of the NPs did not change much (Data not shown). These data support the observation that argon plasma treatment controls the shape of NPs, while precursor amounts controlled the size of the NPs that are formed. Therefore, it can be concluded that larger amounts of starting materials from either higher concentration of solution or larger droplet volumes decrease the efficiency of NP synthesis. As a result, limiting the amount of starting material is key to synthesizing NPs. After analyzing the effects of droplet volume on NP size, it was determined that droplets with volumes ranging from 50 to 500 μL had no significant change in the size or size

distribution of the three different types of NPs synthesized under optimal reduction conditions. The sizes for both AuNPs and AgNPs were consistent at around 40 – 80 nm, while the size of the CuNPs remained at 40 x 160 nm (Table 2). Droplet volumes of more than 500 μL resulted in much larger (5 times) NP sizes (Table 2). In some cases, the size of the particles also reached up to 1 μm . As for droplet size, with droplets larger than 500 μL , we observed an increasing solvent evaporation time. The droplet volume shrank before it froze, which caused the amount of precursor to increase in that given area, thus resulting in larger particle sizes for a similar reason as the concentration increase.

Solvent evaporation is a critical step in plasma-assisted reduction of metal precursors and required 3 minutes of exposure to the vacuum pump. As already demonstrated, NP synthesis is affected by droplet concentration and droplet size. Another crucial factor yet to be addressed involves the dispersion of droplets onto the substrate. In the previous experiments, hydrophobic polystyrene 6-well plates were used for NP synthesis. To help understand how a hydrophilic (plasma-treated polystyrene 6-well plate) substrate may influence the synthesis of NPs, 72 droplets of the 2 mM metal precursor solutions were pipetted onto the substrate and treated under optimal experimental conditions. As expected, the 72 droplets placed onto the hydrophilic substrate demonstrated increased surface wettability and the individual droplets were no longer visible. Instead, a thin layer of solution covered the entire substrate. When comparing the solvent evaporation processes for both hydrophobic and hydrophilic substrates, there was no change in time. In addition, optimal argon plasma treatment conditions were able to completely reduce metal precursors, while maintaining the same NP size and shape (Data not shown). Therefore, it can be concluded that surface wettability does not affect NP synthesis. In another

experiment, the rate of solvent evaporation on NP synthesis was tested by increasing the solvent evaporation time to 150 minutes. This was accomplished by using a less powerful pump. Results from this experiment demonstrate that increasing the solvent evaporation rate causes no significant change in NP size or shape.

3.6. Proposed reduction mechanism for nanoparticle synthesis

NP formation in the form of self-assembly after nucleation is a slow and gradual process that follows a complex mechanism when subjected to cold plasma.^[33,51-53] The electric field of the argon plasma initiates the self-assembly mechanism, and consequently, controls the size and shape of the NPs produced in this study. More specifically, as nucleation occurs, some atoms, once exposed to the electric field, become activated. These activated atoms then induce an activated region, and from this a domino effect ensues, resulting in crystal growth until destabilization occurs.^[27-30] In the first step of NP synthesis, metal precursors (AgNO_3 and CuSO_4) are prepared for nucleation by argon plasma-induced dissociation. This is accomplished by plasma electrons and excited argon species. As bondings are disrupted, the non-metal ions are oxidized and etched away in the form of O_2 , NO_x , H_2O , and SO_x .^[37,39,55] Once the anions are removed, a Coulomb interaction between the electrons and metal precursor ions occurs, facilitating a fast nucleation process, followed by self-assembly, which results in smaller and more stable NPs when compared to conventional plasma reduction methods.^[37-39,56]

The synthesis of AuNPs from the solvent-free gold(III) chloride followed a different and more complex reduction mechanism similar to that of the plasma|liquid interaction, where electrons and hydrogen radicals dominate the reaction. First, an enhanced energy transfer is induced from the plasma species to the catalyst surface by reactions with

electrons and excited argon species.^[37,55,56] From this interaction, hydrogen radicals are generated through the dissociation of the acidic proton via electron collisions.^[37,55] The synergistic effects from both the electrons and the dissociated hydrogen radicals are capable of reducing the chlorinated gold complex through removal of the chlorine ligands. It has been reported that electron-assisted reduction through plasma treatment leads to a more effective reduction of metal complexes containing chlorine atoms when compared to reduction with borohydride or other wet chemical reducing agents.^[56] This is due to the direct transfer of the abundant electrons in the plasma to metal ions.^[56] This synergy between hydrogen radicals and electrons results in a much quicker reduction process than that of both AgNPs and CuNPs. Upon nucleation, the atoms that are formed undergo self-assembly until destabilization occurs.^[37-39,56]

The differences between placing a salt directly into the plasma chamber for ion reduction and our evaporation approach are significant. For example, the evaporation approach (1) controls the amount of starting metal precursor; (2) minimizes nanoparticle aggregation, and (3) increases susceptibility of the metal precursor to argon plasma reduction. More specifically, in the direct salt reduction approach, the water and sulfate ligands of the copper complex form a stable shield that protects Cu^{2+} ion from argon plasma reduction. In order to efficiently reduce the metal ion, argon plasma must first etch away the ligands prior to Cu^{2+} reduction. On the other hand, when using the evaporation approach, the dissolved copper sulfate forms the $[\text{Cu}(\text{OH}_2)_6]^{2+}$ complex and keeps the metal ion in a well distributed form.^[59] As a result, the water ligands can be easily etched away, therefore, creating ion separation, which allows for better exposure of the metal ion to the argon plasma. Consequently, the evaporation process results in slower nucleation,

but facilitates nanoscale particles using self-assembly during the ion reduction process. The controlled environment of low-temperature, low-pressure argon plasmas show reproducible characteristics including shape, particle size, particle agglomeration, and stability when compared to traditional thermal methods.^[37,39,57]

4. Conclusion

In this study, the reduction of cations to produce AgNPs, AuNPs, and CuNPs was accomplished using argon plasma chemistry and self-assembly. More specifically, we were able to utilize a low-temperature, low-pressure argon-plasma approach for the reduction of both noble and non-noble cations. Nucleation and crystal growth studies reveal that the synthesis of the metal NPs could be accomplished within 150 seconds of argon plasma treatment, with efficiency rates upwards of 98%. When characterized using SEM and UV/Vis, the results confirm the presence of metal NPs. Using microscopy analysis, AgNPs were round-shaped, with a sizes of 40 – 80 nm, while AuNPs were hexagon-shaped, with sizes of 40 – 80 nm, and CuNPs were found to possess a rod-shape, with sizes of 40 nm by 160 nm. These results demonstrate that the argon plasma method utilized in our lab is rapid, ecofriendly, and a versatile reduction approach for the synthesis of both noble and non-noble metal NPs. From the viewpoint of green chemistry principals, electrons produced from plasma are among the best reducing agents.^[56,58] According to the energy balance, this electron-induced reduction technique significantly reduces energy consumption, economic cost as well as emissions of toxic or hazardous materials.^[56] On the other hand, most chemical reducing agents are hazardous to both the human body and the environment. The byproducts associated with wet chemistry methods are also not cheap, since many types of waste are generated and require special disposal. Different applications of plasma

technology are currently being explored for synthesis of unique compounds such as sulfides, nitrides, and phosphides under mild conditions.^[58] In addition, plasma is a useful alternative for oxidation, reduction, decomposition, surface cleaning, surface treatment, template removal, etching, doping, coating, alloying, and others.^[56-58] Cold plasmas are also attracting more attention for catalyst preparation with thermally sensitive substrates such as porous polymers, biomolecules, nanosized zeolites, and ultrahigh-surface-area catalysts.^[56,58]

Author contributions

Marjan Darwish – Synthesis of nanoparticles and UV/vis

Camila Mafla-Gonzalez – Synthesis of nanoparticles and UV/vis

Belmin Kolenovic – Synthesis of nanoparticles and UV/vis

Adrianna Deremer – Synthesis of nanoparticles and UV/vis

Daniel Centeno – SEM imaging

Tianchi Liu – SEM imaging/TEM elemental analysis

Deok-Yang Kim – TEM elemental analysis

Thomas Cattabiani – Synthesis of nanoparticles, SEM analysis, and editor

Thomas J. Drwiega – UV/vis analysis and editor

Ish Kumar – Optimization of NP synthesis conditions

Clive Li – Analysis of NP size and shape

Christian Traba – Corresponding Author

Acknowledgements

This work was supported by National Institutes of Health (NIH grant EB029710). Dr.

Christian Traba was also awarded a Research Fellowship from Fairleigh Dickinson University.

Conflicts of interest disclosure statement

The authors declare no potential conflicts of interest.

Figure legends

Figure 1. Schematic diagram of the plasma chamber, with a (1) Pyrex reaction chamber, (2) semitubular electrode, (3) gas inlet, (4) RF power supply, (5) sample holder (8 cm from gas inlet), and (6) vacuum connection.

Figure 2. Real time images of the low-temperature, low-pressure NP synthesis process starting with either 2 mM silver nitrate (X), gold(III) chloride (Y), or copper(II) sulfate (Z). First, (A) 72 droplets (50 μ L) are carefully placed onto the polystyrene sample holder. Next, (B) the sample holder is placed into the plasma chamber and the vacuum is turned on. Once exposed to the vacuum the evaporation process begins (C). At approximately 220 mtorr, (D) the evaporation process is complete and a salt is left behind (E). Once the chamber reaches 220 mtorr, the plasma is turned on (F) and set to optimal experimental conditions. After argon plasma treatment, NPs are synthesized (G), and the sample holders are removed from the plasma device, collected, and then washed.

Figure 3. Schematic diagram of the low-temperature, low-pressure argon plasma reduction process beginning with (A) placement of 72 (50 μ L) droplets of either 2 mM silver nitrate, Gold(III) chloride, or copper(II) sulfate solutions onto a polyethylene 6-well plate, followed by subsequent exposure to vacuum (B), resulting in solvent evaporation (C), and

then exposure to optimal argon plasma experimental conditions (E), resulting in the synthesis of NPs (F).

Figure 4. Images (A) of AgNPs (left), AuNPs (middle), and CuNPs (right) synthesized in this study and placed into 5-inch test tubes after washing and collection. Before (L) and after (R) images of 2 mM solutions of (B) silver nitrate, (C) Gold(III) chloride, and (D) copper(II) sulfate treated with optimal argon plasma treatment to form corresponding AgNPs, AuNPs, and CuNPs. Images of the sonicated colloidal solutions were taken two days after synthesis.

Figure 5. Effects from (A) argon plasma power, and (B) argon plasma treatment time were studied to understand the nucleation and crystal growth behind NP synthesis. When studying argon plasma power, exposure times were fixed at 5, 60, and 150 seconds for gold, silver, and copper, respectively. When dealing with argon plasma treatment time, argon plasma powers were fixed at 80 W. Amounts of NPs that were synthesized were calculated using an analytical balance. Data represent the mean and SD of at least five hundred samples.

Figure 6. Ultraviolet-visible spectra of (A) AgNPs, (B) AuNPs, and (C) CuNPs, with corresponding SEM images of (D) AgNPs, (E) AuNPs, and (F) CuNPs, when deposited on silica wafers. Scale bars are 20 nm. The applied voltage was 3 kV.

Figure 7. TEM elemental analysis, with corresponding EDS and the elemental frequencies of (A) AgNPs, (B) AuNPs, and (C) CuNPs, deposited on a 300 mesh copper TEM grid. The data was analyzed using image processing software called EDAX Team EDS.

Figure 8. Effects from (A) droplet concentration, (B) droplet volume were studied to understand the nucleation and crystal growth behind NP synthesis. When studying droplet

concentration, volume of the droplets was fixed 50 μL during exposure to optimal experimental conditions. When dealing with droplet volume, concentration of the droplets was fixed to 2 mM and plasma treatment was kept under optimal experimental conditions. Amounts of NPs that were synthesized were calculated using an analytical balance. Data represent the mean and SD of at least five hundred samples. TEM analysis (C) of (1) AgNPs, (2) AuNPs, and (3) CuNPs. AgNPs and AuNPs were synthesized using 50 μL droplets with concentrations of 40 mM, while CuNPs were synthesized using 50 μL droplets with 20 mM. NPs were deposited on a 300 mesh copper TEM grid. Scale bars for TEM imaging are 100 nm.

Table 1. When studying the effects of droplet concentration on NP size, the volume of the droplets was fixed at 50 μL , while changing droplet concentration and exposing the metal precursor to optimal experimental conditions. Units for NP size are in nm.

Table 2. When studying the effects of droplet volume on NP size, the concentration of the droplets was fixed at 2 mM, while changing droplet volume and exposing the metal precursor to optimal experimental conditions. Units for NP sizes are in nm.

References

1. Chairuangkitti, P., Lawanprasert, S., Roytrakul S., et al. Silver nanoparticles induce toxicity in A549 cells via ROS-dependent and ROS-independent pathways. *Toxicology in Vitro*. 2013; 27(1): 330–338.
2. Huh, A.J., Kwon, Y.J., “Nanoantibiotics”: A new paradigm for treating infectious diseases using nanomaterials in the antibiotics resistant era. *J. Control Release*. 2011; 156: 128–145.

3. Prabhu, S., Poulouse, E.K. Silver nanoparticles: mechanism of antimicrobial action, synthesis, medical applications, and toxicity effects. *International Nano Letters*. 2012; 2(1): 1–10.
4. Marassi, V., Di Cristo, L., Smith, S.G.J., Ortelli, S., Blosi, M., Costa, A.L., Reschiglian, P., Volkov, Y., Prina-Mello, A. Data from: Silver nanoparticles as a medical device in healthcare settings: a five-step approach for candidate screening of coating agents. *R. Soc. Open Sci.* 2018; 31;5(1):171113.
5. Rai, M.K., Deshmukh, S.D., Ingle, A.P., Gade, A.K. Silver nanoparticles: the powerful nanoweapon against multidrug-resistant bacteria. *J. Appl. Microbiol.* 2012; 112(5): 841–852.
6. Wang, Z., Zhu, Y. A simple plasma reduction for the synthesis of Au and Pd nanoparticles at room temperature. *Chinese J. of Chem. Eng.* 2015; 23: 1060-1063.
7. Yeh, Y.C., Creran, B., Rotello, V.M. Gold Nanoparticles: Preparation, Properties, and Applications in Bionanotechnology. *Nanoscale*. 2012; 4: 1871–1880.
8. Doane, T.L., Burda, C. The Unique Role of Nanoparticles in Nanomedicine: Imaging, Drug Delivery and Therapy. *Chem. Soc. Rev.* 2012; 41: 2885.
9. Doria, G., Conde, J., Veigas, B., Giestas, L., Almeida, C., Assunção, M., Rosa, J., Baptista, P.V. Noble Metal Nanoparticles for Biosensing Applications. *Sensors*. 2012; 12: 1657–1687.
10. Li, N., Zhao, P., Astruc, D. Anisotropic Gold Nanoparticles: Synthesis, Properties, Applications, and Toxicity. *Angew. Chemie Int. Ed.* 2014; 53: 1756–1789.

11. Puliyalil, H., Jurković, D.L., Dasireddy V.D.B.C., Likozar, B. A review of plasma-assisted catalytic conversion of gaseous carbon dioxide and methane into value added platform chemicals and fuels. *RCS Advances*. 2018; 8: 27481-27508.
12. Jurković, D.L., Puliyalil, H., Pohar, A., Likozar, B. Plasma-activated methane partial oxidation reaction to oxygenate platform chemicals over Fe, Mo, Pd and zeolite catalysts. *Int. J. Energy Res.* 2019; 43: 8085–8099.
13. Nagar, N., Devra, V. Green synthesis and characterization of copper nanoparticles using *Azadirachta indica* leaves. *Mater. Chem. Phys.* 2018; 213: 44–51.
14. Rajesh, K., Ajitha, B., Reddy, Y.A.K., Suneetha, Y., Reddy, P.S. Assisted green synthesis of copper nanoparticles using *Syzygium aromaticum* bud extract: Physical, optical and antimicrobial properties. *Optik*. 2018; 154: 593–600.
15. Begletsova, N., Selifonova, E., Chumakov, A.; Al-Alwani, A.; Zakharevich, A.; Chernova, R.; Glukhovskoy, E. Chemical synthesis of copper nanoparticles in aqueous solutions in the presence of anionic surfactant sodium dodecyl sulfate. *Colloids Surf. Physicochem. Eng. Asp.* 2018; 552: 75–80.
16. Irvani, S., Korbekandi, H., Mirmohammadi, S.V., Zolfaghari, B. Synthesis of silver nanoparticles: chemical, physical and biological methods. *Res. Pharm. Sci.* 2014; 9(6): 385–406.
17. Nagy, A., Harrison, A., Sabbani, S., Munson, R.S., Dutta, P.K., Waldman, W.J. Silver nanoparticles embedded in zeolite membranes: release of silver ions and mechanism of antibacterial action. *Int. J. Nanomed*, 2011; 6: 1833-1852.

18. Lu, Y., Liu, G.L., Lee, L.P. High-Density Silver Nanoparticle Film with Temperature-Controllable Inter-particle Spacing for a Tunable Surface Enhanced Raman Scattering Substrate. *Nano Lett.* 2005; 5(1): 5–9.
19. Zhu, X., Huo, P., Zhang, Y.P., Liu, C.J. Characterization of Argon Glow Discharge Plasma Reduced Pt/Al₂O₃ Catalyst. *Ind. Eng. Chem. Res.* 2006; 45(25): 8604–8609.
20. Bromberg, V., Ma, S., Egittob, F.D., Singler, T.J. Highly conductive lines by plasma-induced conversion of inkjet-printed silver nitrate traces. *J. Mater. Chem. C.* 2013; 1: 6842–6849.
21. Zou, J.J., Zhang, Y.P., Liu, C.J. Reduction of Supported Noble-Metal Ions Using Glow Discharge Plasma. *Langmuir.* 2006; 22(26): 11388–11394.
22. Crowther, J.M., Badyal, J.P.S. Cold Plasma Metallization of Supported Metal Salt Layers. *Aust. J. Chem.* 2012; 65: 1139–1144.
23. Yu, Y., Li, Y., Pan, Y., Liu, C.J. Fabrication of palladium/graphene oxide composite by plasma reduction at room temperature. *Nanoscale Res. Lett.* 2012; 7(1): 234–238.
24. Osonio, A.P., Vasquez, M.R. Plasma-assisted reduction of silver ions impregnated into a natural zeolite framework. *Applied Surface Science.* 2018; 432: 156–162.
25. Gunawan, P., Guan, C., Song, X., Zhang, Q., Leong, S.S.J., Tang, C., Chen, Y., Chan-Park, M.B., Chang, M.W., Wang, K., Xu, R. Hollow Fiber Membrane Decorated with Ag/MWNTs: Toward Effective Water Disinfection and Biofouling Control. *ACS Nano.* 2011; 5: 10033-10040.
26. Li, X., Lenhart, J.J. Aggregation and Dissolution of Silver Nanoparticles in Natural Surface Water. *Environ. Sci. Technol.*, 2012; 46: 5378-5386.

27. Shevchenko, E.V., Talapin, D.V., Kotov, N.A., O'Brien, S., Murray, C.B. Structural diversity in binary nanoparticle superlattices. *Nature*. 2006; 439: 55-59.
28. Bigioni, T.P., Lin, X.M., Nguyen, T.T., Corwin, E.I., Witten, T.A., Jaeger, H.M. Kinetically driven self assembly of highly ordered nanoparticle monolayers. *Nat. Mater.* 2006, 5(4): 265-270.
29. Pierrat, S., Zins, I., Breivogel, A., Sonnichsen, C. Self-Assembly of Small Gold Colloids with Functionalized Gold Nanorods. *Nano Lett.* 2007, 7(2): 259-263
30. Chen, S. H., Fan, Z. Y., Carroll, D. L., Silver Nanodisks: Synthesis, Characterization, and Self-Assembly. *J. Phys. Chem. B.* 2002; 106(42): 10777-10781.
31. Bruggeman, P., and Leys, C. Non-thermal plasmas in and in contact with liquids. *J. Phys. D: Appl. Phys.* 2009; 42: 053001.
32. Wang, D, Zou, Y., Tao, L., Zhang, Y., Liu, Z., Du, S., Zang, S., Wand, S. Low-temperature plasma technology for electrocatalysis. *Chin. Chem. Lett.* 2019; 30: 826-38.
33. Dou, S., Wang, X., Wang, S. Rational design of transition metal-based materials for highly efficient electrocatalysis. *Small Methods.* 2019; 3: 1800211.
34. Gubkin, J., Elektrolytische Metallabscheidung an der freien Oberfläche einer Salzlösung. *Ann. Phys. Chem.* 1887; N.F. 32 Ž9.Ž1887. 114.
35. Kareem, T.A., Kaliani, A.A. Glow discharge plasma electrolysis for nanoparticles synthesis. *Ionics.* 2012; 18: 315–327. <https://doi.org/10.1007/s11581-011-0639-y>.
36. Graham, W.G., Stalder, K.R. Plasmas in liquids and some of their applications in nanoscience. *J. Phys. D.: Appl. Phys.* 2011; 44: 1206 (174037):8. doi:10.1088/0022-3727/44/17/174037.

37. Wang, Z., Zhang, Y., Neyts, E.C., Cao, X., Zhang, X., Jang, B.W.-L., Liu, C. Catalyst preparation with plasmas: how does it work? *ACS Catal.* 2018; 8: 2093-110.
38. Di, L., Zhang, J., Zhang, X., Wang H., Ji, H., Li, Y., Bu, D. Cold plasma treatment of catalytic materials: a Review. *J. Phys. D: Appl. Phys.* 2021; 54: 333001.
39. Di, L., Zhang, J., Zhang, X. A review on the recent progress, challenges, and perspectives of atmospheric-pressure cold plasma for preparation of supported metal catalysts. *Plasma Process Polym.* 2018; 15:e1700234.
<https://doi.org/10.1002/ppap.201700234>.
40. He, P., Liu, H., Li, Z., Liu, Y., Xu, X., Li, J. Electrochemical deposition of silver in room temperature ionic liquids and its surface enhanced Raman scattering effect. *Langmuir.* 2004; 20(23):10260–10267. doi:10.1021/la0484801.
41. Vennekamp, M., Janek, J. Control of the surface morphology of solid electrolyte films during field driven growth in a reactive plasma. *Phys. Chem. Chem. Phys.* 2005; 7: 666–677.
42. Vennekamp, M., Janek, J. Plasma electrochemical growth of ion-conducting AgBr and AgCl. *Solid State Ionics.* 2001; 141/142, 71– 80.
43. Xie, Y.B., Liu, C.J. Stability of Ionic Liquids under the Influence of Glow Discharge Plasmas *Plasma Process. Polym.* 2008; 5: 239–245.
44. Polidor, D., Brito, G., Roca, J., Sciorra, L., Li, C., Traba, C. Can the Argon Plasma “Grafting-From” Approach Be Used For The Modification of Nanoparticle Systems, *Colloid and Interface Science Communications*, 2020, 37: 100269.
45. Badiei, Y., Traba, C., Rosales, R., Vera, C., Lopez-Rojas, A., Amaya, C., Shahid, M., Concepcion, JJ. Plasma-Initiated Graft Polymerization of Acrylic Acid onto Fluorine-

Doped Tin Oxide Electrodes as a Platform for the Immobilization of Water-Oxidation Catalysts, *ACS Materials and Interfaces*. 2021; 13(12): 14077-90.

46. Ambi, A., Vera, C., Borbon, K., Bryan, J., Parikh, N., Perez, N., Rojas, AL., Kumar, S., Stradford, C., Traba, C. Plasma-initiated Graft Polymerization as an Immobilization Platform for Metal Free Russian Propolis Ethanol Extracts Designed Specifically for Biomaterials. *Biofouling*. 2018; 34(5): 557-568.

47. Ambi, A., Parikh, N., Vera, C., Burns, K., Montano, N., Sciorra, L., Epstein, J., Zeng, D., Traba, C. Anti-infection Silver Nanoparticle Immobilized Biomaterials Facilitated by Argon Plasma Grafting Technology, *Biofouling*, 34: 3; 2018; 273-286.

48. Liu, T., Stradford, C., Ambi, A., Roca, J., Cattabiani, T., Drwiega, T., Li, C., Traba C. Plasma-initiated Graft Polymerization of Carbon Nanoparticles as Nano-Based Drug Delivery Systems. *Biofouling*. 2021; 38(1), 13-28.

49. Zhou, M., Chen, SH., Zhao, SY. Preparation of branched gold nanocrystals by an electrochemical method, *Chem. Lett*. 2006: 35: 332–333.

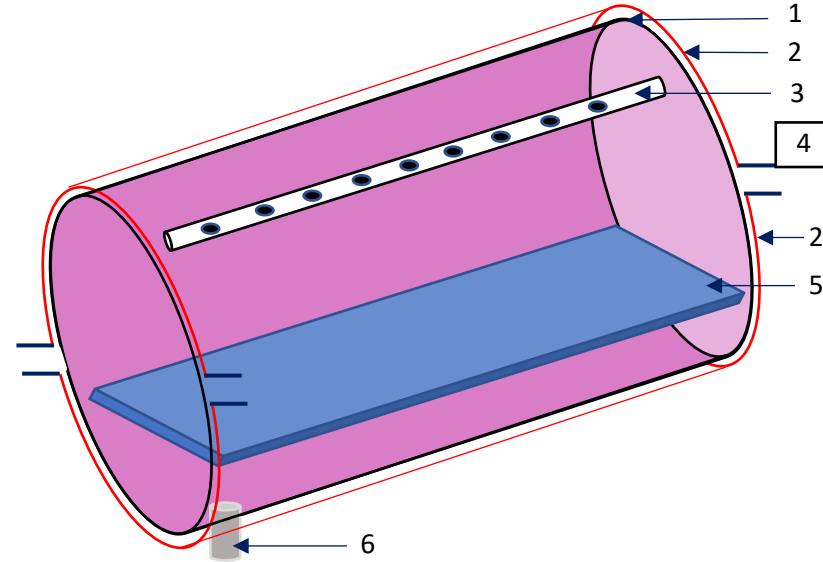
50. Chan, SC., Barteau, MA. Preparation of highly uniform Ag/TiO₂ and Au/TiO₂ supported nanoparticle catalysts by photodeposition, *Langmuir*. 2005; 21: 5588–5595.

51. Chen, Y., Wang, H., Liu, CJ., Zeng, Z., Zhang, H., Zhou, C., Jia, X., Yang, Y. Formation of monometallic au and pd and bimetallic au–pd nanoparticles confined in mesopores via ar glow-discharge plasma reduction and their catalytic applications in aerobic oxidation of benzyl alcohol, *J. Catal*. 2012; 289: 105–117.

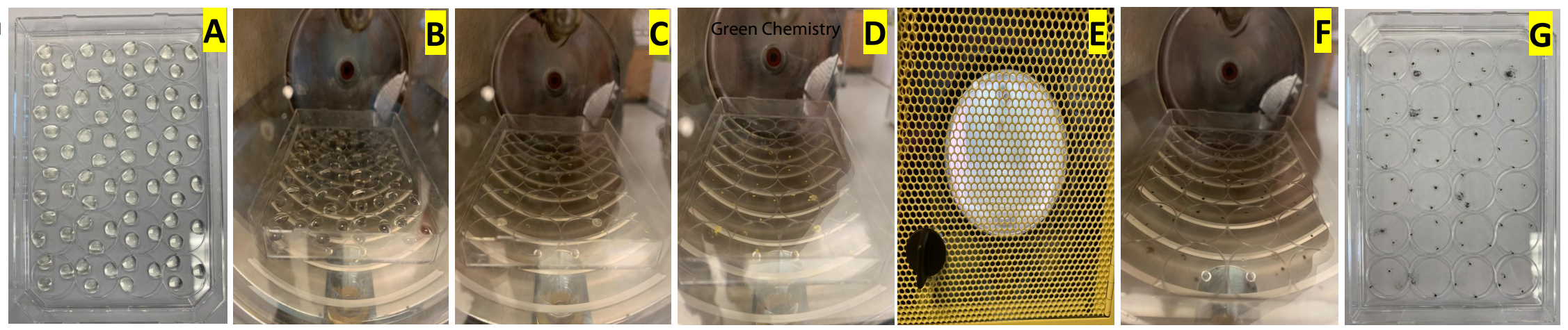
52. Deol, S., Weerasuriya, N., Shon, YS. Stability, cytotoxicity and cell uptake of water-soluble dendron–conjugated gold nanoparticles with 3, 12 and 17 nm cores. *J. Mater. Chem. B*. 2015; 3: 6071-6080.

53. Nguyen, LN., Kaushik, N., Lamichhane, P., Mumtaz, S., Paneru, R., Bhartiya, P., Kwon, JS., Mishra, YK., Nguyen, LQ., Kaushik, NK., Choi, EH. In-situ plasma-assisted synthesis of polydopamine-functionalized gold nanoparticles for biomedical applications. *Green Chemistry*. 2020; 22: 6588-6599.
54. Ramyadevi, J., Jeyasubramanian, K., Marikani, A., Rajakimar, G., Rahuman, AA. Synthesis and antimicrobial activity of copper nanoparticles. *Materials Letters*. 2012; 71: 114-116.
55. Kaneko, T., Baba, K., Harada, T. Hatakeyama, R Novel Gas-Liquid Interfacial Plasmas for Synthesis of Metal Nanoparticles. *Plasma Process. Polym.* 2009; 6: 713–718.
56. Liu, C., Zhao, Y., Li, Y., Zhang, D., Chang, Z., Bu, X. Perspectives on electron-assisted reduction for preparation of highly dispersed noble metal catalysts. *ACS Sustain. Chem. Eng.* 2013; 2: 3-13.
57. Patel, J., Němcová, L., Maguire, P., Graham, W.G., Mariotti, D. Synthesis of surfactant-free electrostatically stabilized gold nanoparticles by plasma-induced liquid chemistry. *Nanotechnology*. 2013; 24: 245604.
58. Liu, C.-J., Li, M. Y., Wang, J.Q., Zhou, X.T., Guo, Q.T., Yan, J.M., Li, Y.Z. Chin. Plasma methods for preparing green catalysts: Current status and perspective. *J. Catal.* 2016; 37: 340–348.
59. Wan, J., Kim, Y., Mulvihill, M.J., Tokunaga, T.K. Dilution Destabilizes Engineered Ligand-Coated Nanoparticles in Aqueous Suspensions. *Environmental Toxicology and Chemistry*. 2018; 37: 1301–1308.

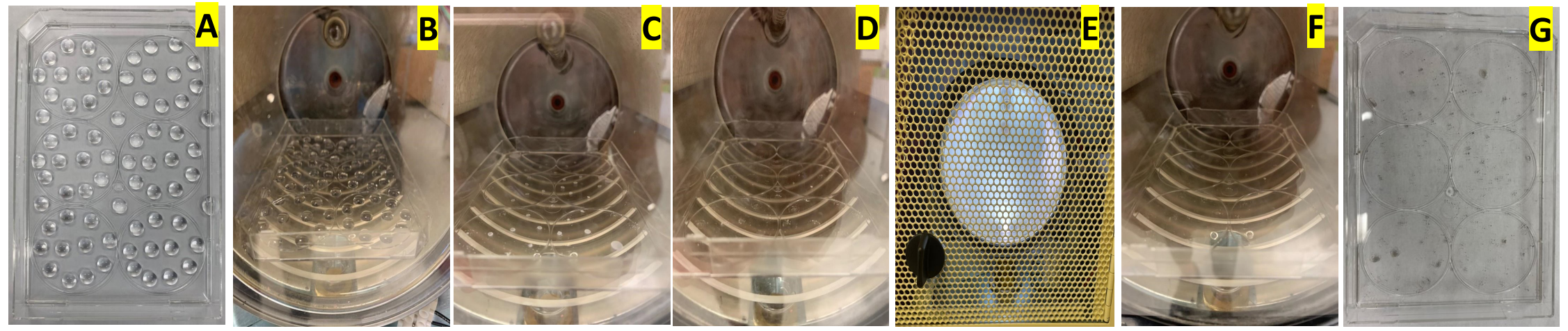
Argon Plasma



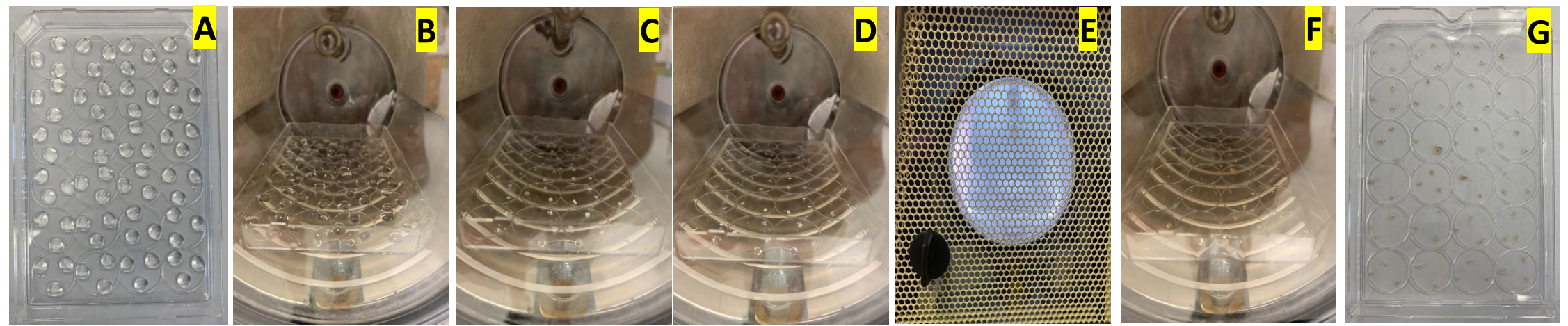
X

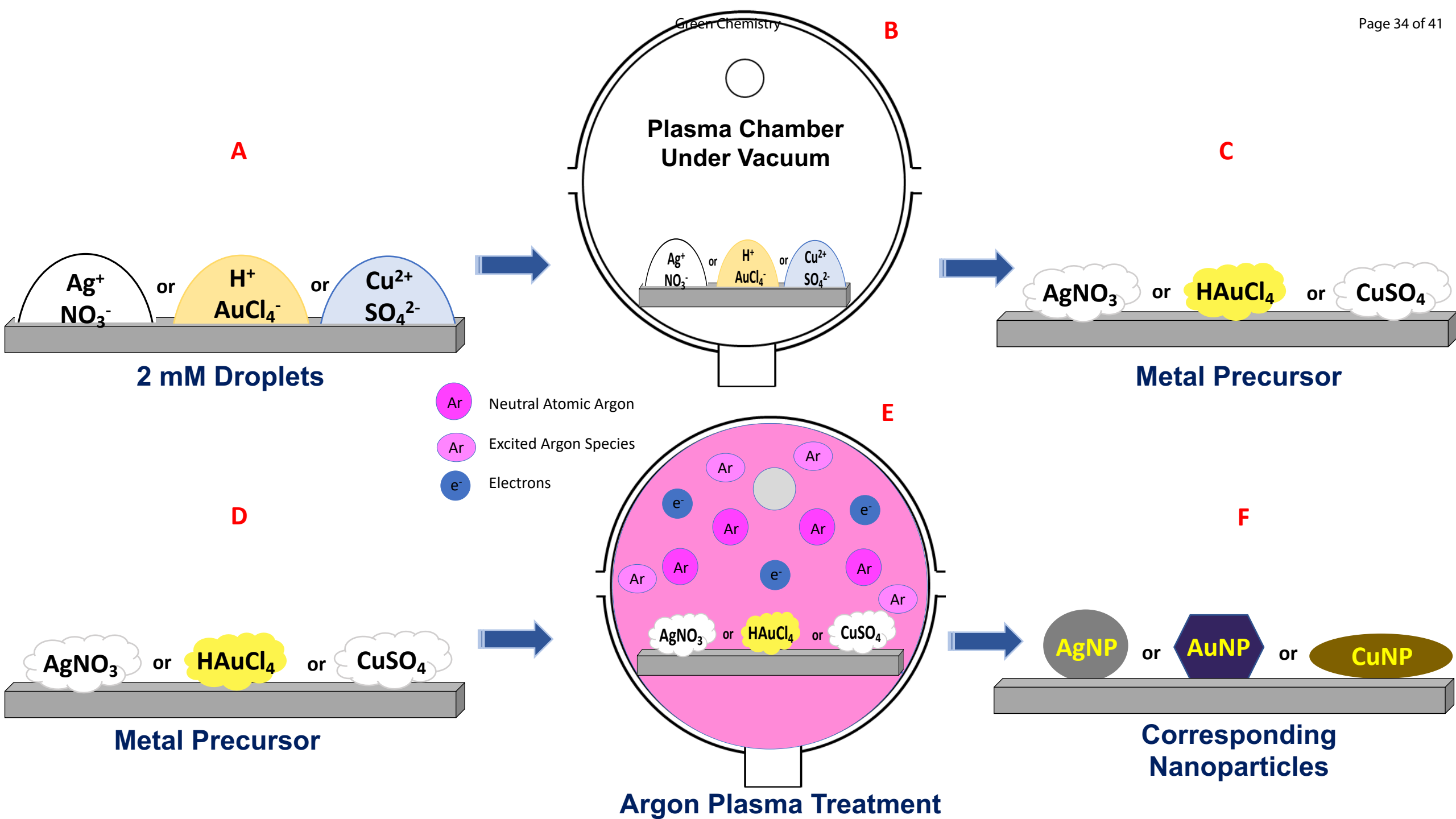


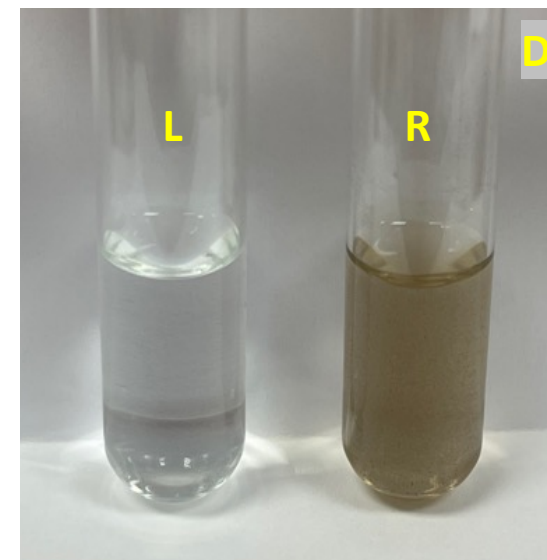
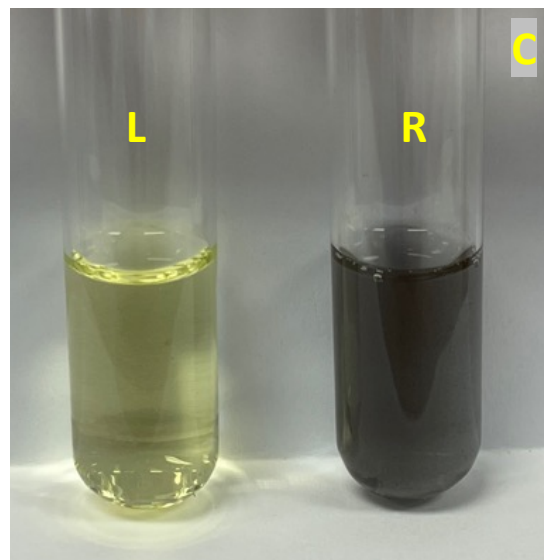
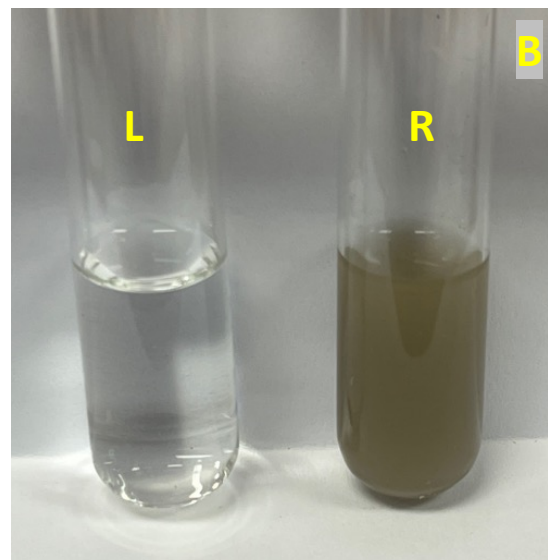
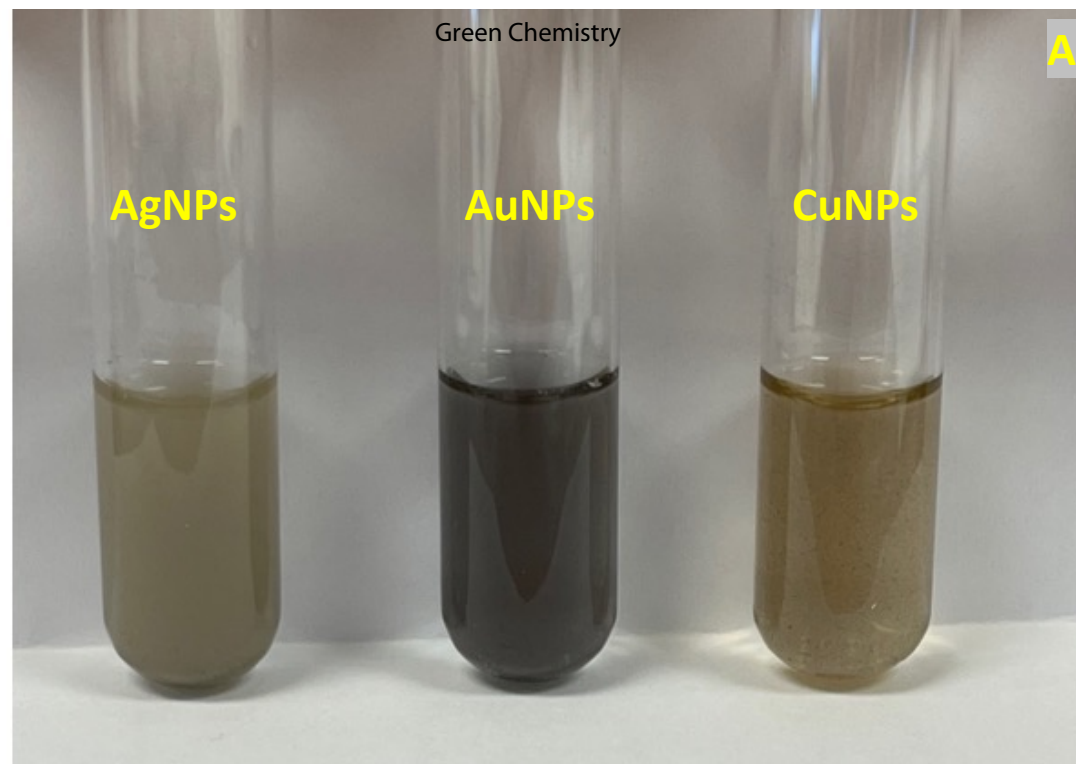
Y

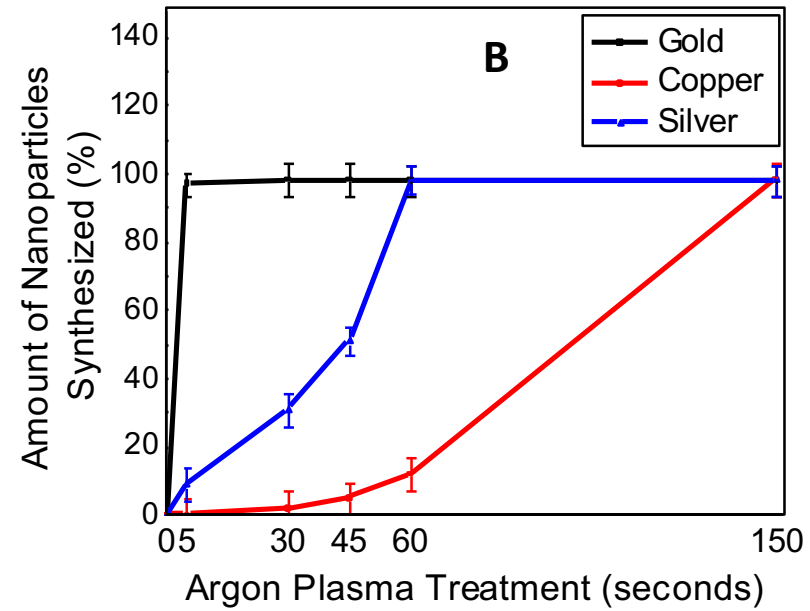
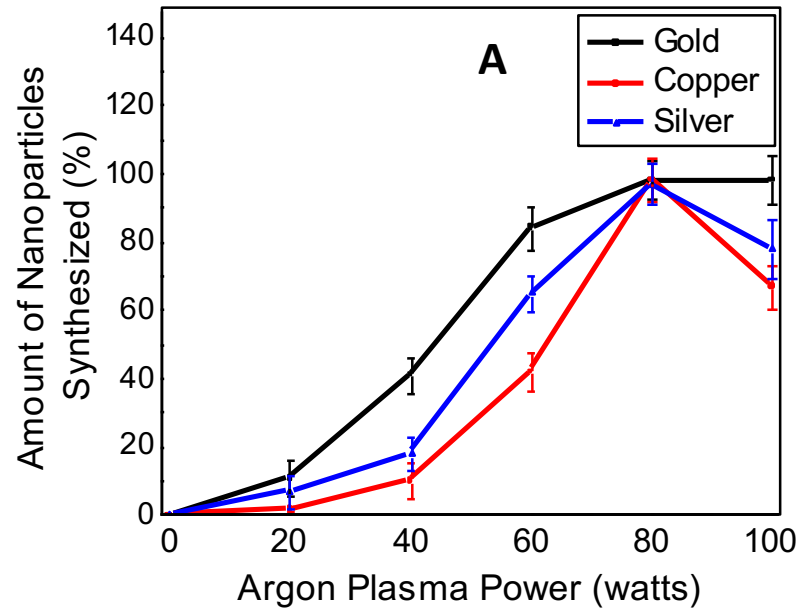


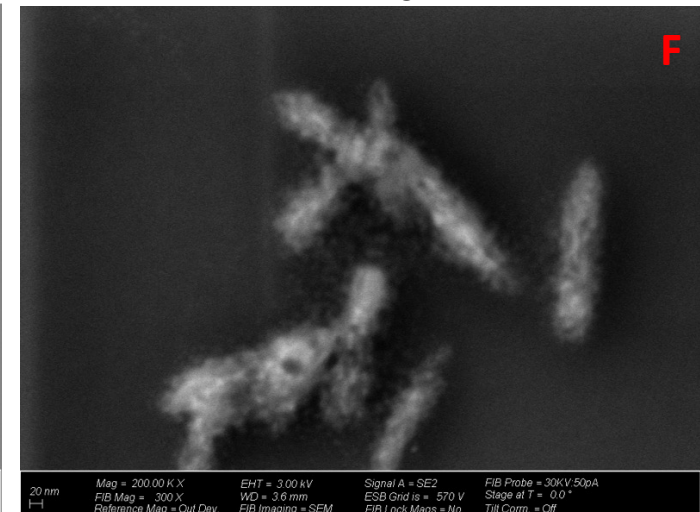
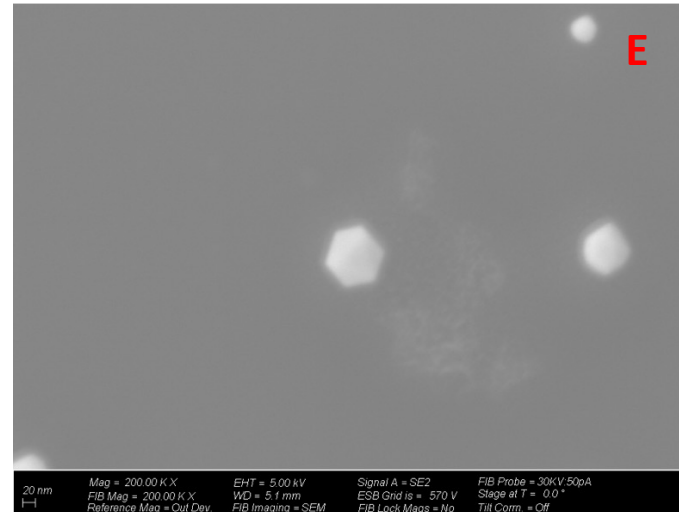
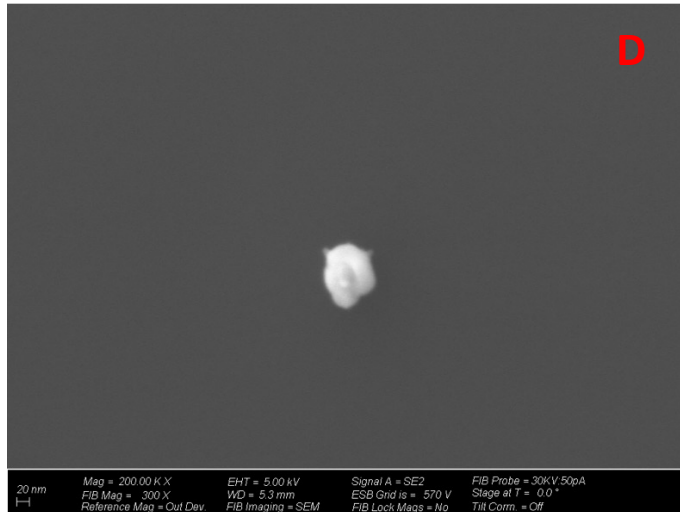
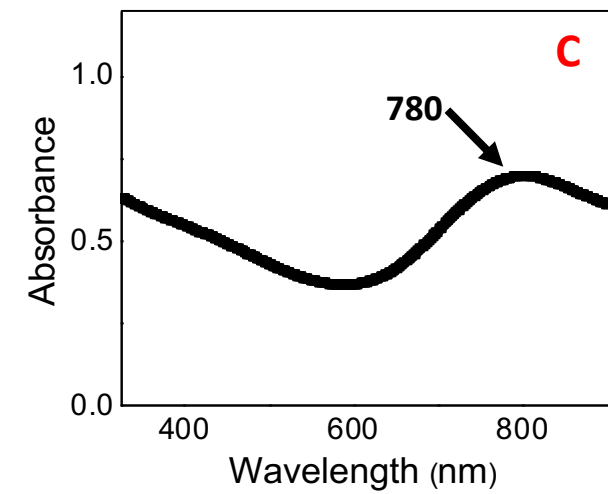
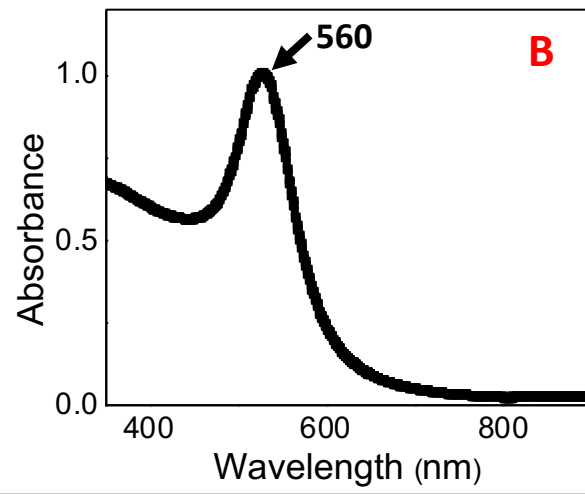
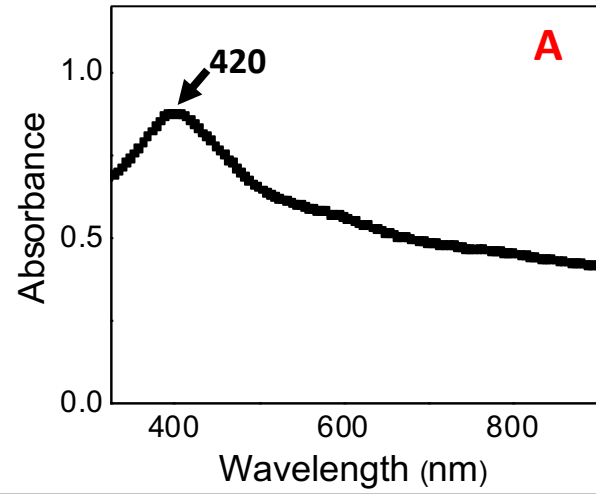
Z



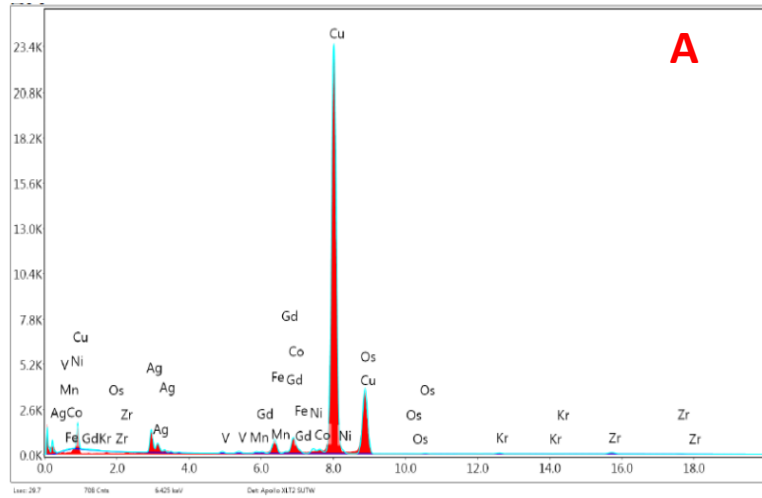








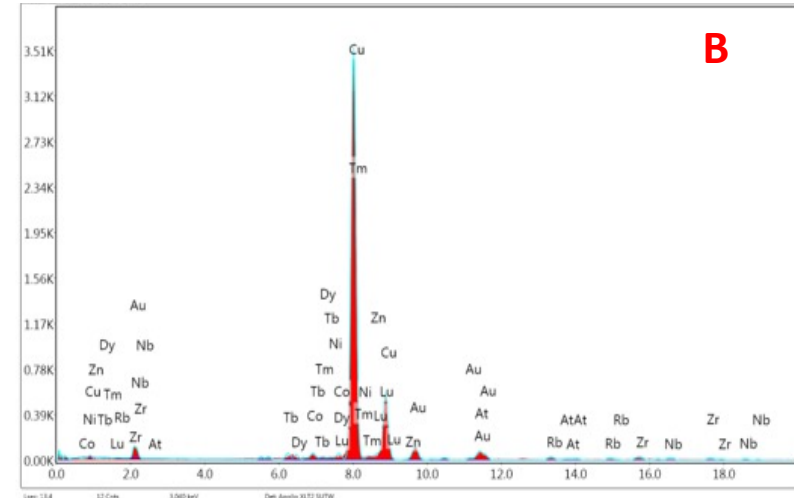
EDAX TEAM EDS



A

Element	Weight %	Atomic %	Xpt	KAB Factor	Net Int.	Net Error %
Ag L	4.79	2.87	0.00	1.51	888.53	1.50
Fe K	2.35	2.71	0.00	0.85	770.14	1.60
Co K	2.90	3.17	0.00	0.90	897.48	1.26
Cu K	89.96	91.25	0.00	1.00	25192.92	0.13
	100.00					

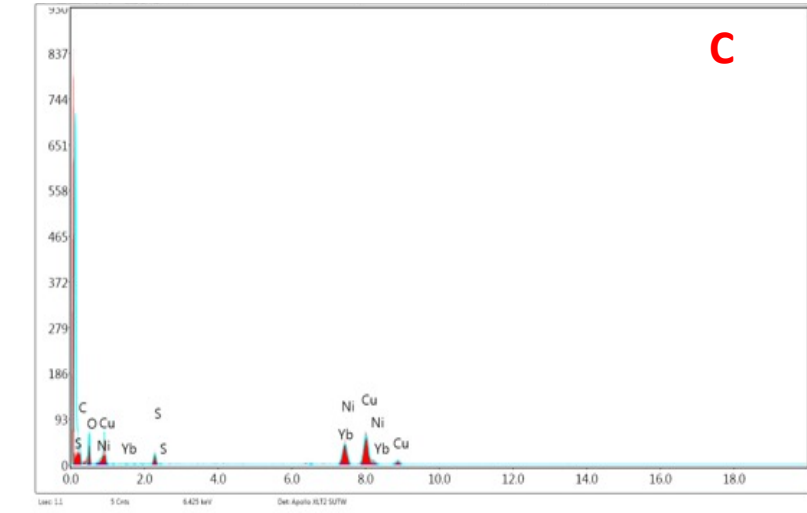
EDAX TEAM EDS



B

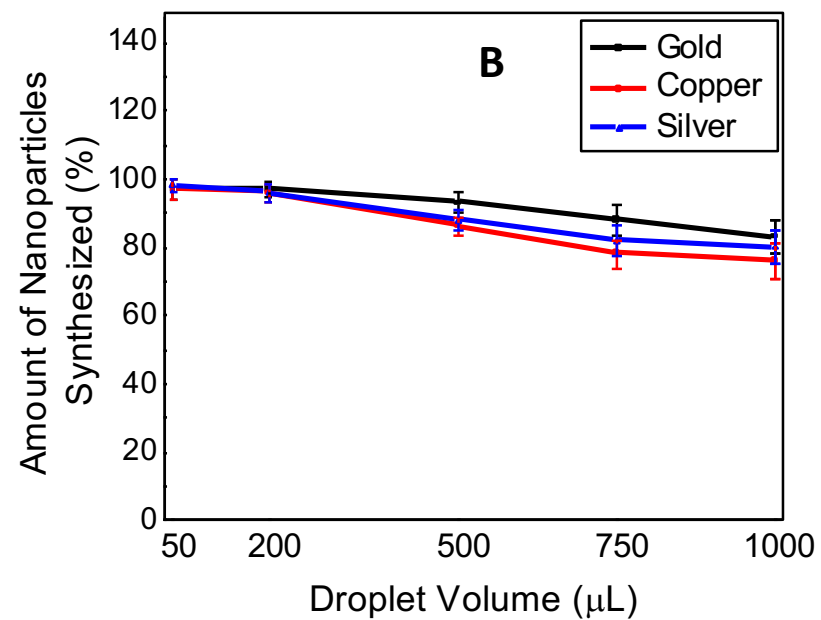
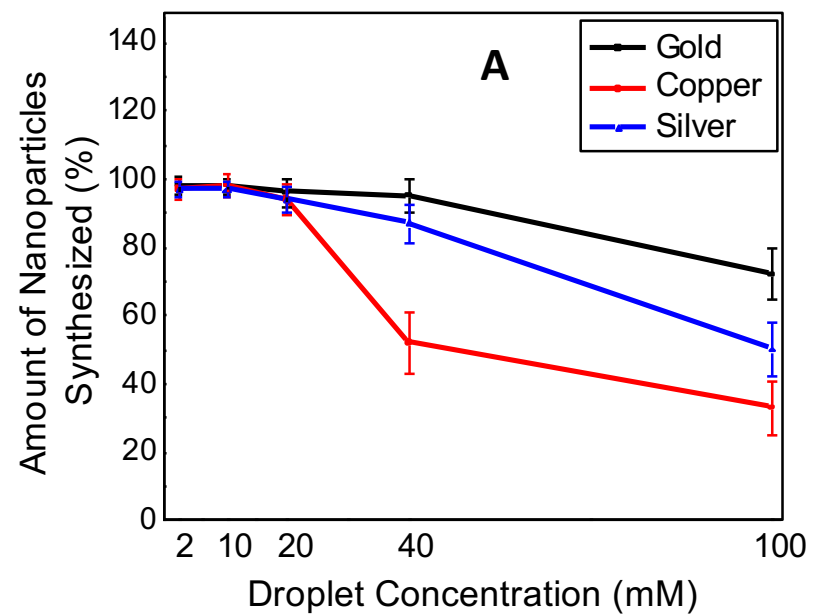
Element	Weight %	Atomic %	Xpt	KAB Factor	Net Int.	Net Error %
Cu K	92.61	96.43	0.00	1.00	8417.53	0.32
Au L	4.49	1.51	0.00	1.30	313.94	4.70
Nb K	2.90	2.07	0.00	4.18	63.08	6.39
	100.00					

EDAX TEAM EDS

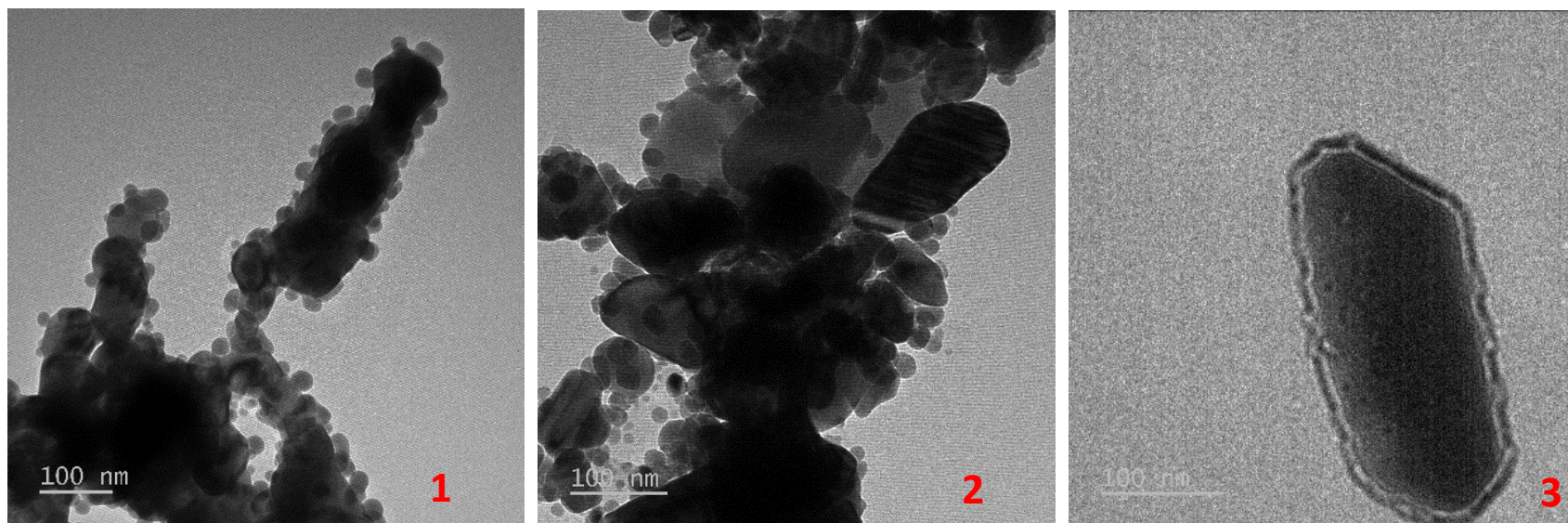


C

Element	Weight %	Atomic %	Xpt	KAB Factor	Net Int.	Net Error %
Cu K	100.00	100.00	0.00	1.00	1803.96	2.91
	100.00					



C



Precursor	2 mM	20 mM	40 mM	60 mM	80 mM	100 mM
HAuCl₃	40 – 80	40 – 80	40 – 80	>250	>450	>500
AgNO₃	40 – 80	40 – 80	40 – 80	>250	>450	>500
CuSO₄	40 x 160	40 x 160	>100 x 500	>300 x 900	>300 x 900	>300 x 900

Precursor	50 μL	200 μL	400 μL	500 μL	700 μL	1000 μL
HAuCl_3	40 – 80	40 – 80	40 – 80	40 – 80	>500	>700
AgNO_3	40 – 80	40 – 80	40 – 80	40 – 80	>500	>700
CuSO_4	40 x 160	40 x 160	40 x 160	40 x 160	>200 x 900	>400 x 1000